Modern Physics Letters B
Vol. 33, No. 0 (2021) 2141006 (17 pages)

DOI: 10.1142/S0217984921410062

Physical impact of thermo-diffusion and diffusion-thermo on Marangoni convective flow of hybrid nanofluid ($MnZiFe_2O_4$–$NiZnFe_2O_4$–H_2O) with nonlinear heat source/sink and radiative heat flux

Ying-Qing Song[*], M. Ijaz Khan[†], Sumaira Qayyum[‡], R. J. Punith Gowda[§], R. Naveen Kumar[§], B. C. Prasannakumara[§], Yasser Elmasry[¶], Yu-Ming Chu[‖,**]

[*] *School of Science, Hunan City University, Yiyang 413000, China*

[†] *Department of Mathematics and Statistics, Riphah International University I-14, Islamabad 44000, Pakistan*

[‡] *Department of Mathematics, Quaid-I-Azam University 45320, Islamabad 44000, Pakistan*

[§] *Department of Studies and Research in Mathematics, Davangere University, Davangere, Karnataka, India*

[¶] *Department of Mathematics, College of Sciences, King Khalid University, Abha 61413, Saudi Arabia*

[‖] *Department of Mathematics, Huzhou University, Huzhou 313000, China*
[**] *chuyuming@zjhu.edu.cn*

Received 28 February 2021
Accepted 5 May 2021
Published

The objective of this study is to illustrate the influence of Marangoni convection, nonlinear heat sink/source, thermal radiation, viscous dissipation, activation energy, Soret and Dufour effects on magnetohydrodynamics flow of nanofluid generated by rotating disk. Further, the entropy generation equation is derived as a function of velocity, concentration, and thermal gradients. The governing equations of the model along with associated boundary constraints are reduced to ordinary differential equations by adopting suitable similarity transformation. Later, these equations are tackled numerically by means of shooting technique. The whole examination is performed by using two distinctive nanoparticles of ferrites in particular, manganese zinc ferrite ($MnZnFe_2O_4$) and nickel zinc ferrite ($NiZnFe_2O_4$) in a carrier liquid ($C_{10}H_{22}$). The physical characteristics of velocity, thermal, concentration entropy generation, skin friction, and Nusselt number against numerous pertinent parameters are discussed in detail and deliberated graphically. Result reveals that thermal gradient shows substantial enhancement for advanced values of heat sink/source parameter. The entropy production increases with

[**] Corresponding author.

an augmentation in the Brinkman number and Marangoni ratio values. The escalation in Marangoni ratio and Dufour number improves the rate of heat transference.

Keywords: Hybrid nanofluid; Marangoni convection; nonlinear thermal radiation and heat sink/source; Soret and Dufour effects; entropy generation.

1. Introduction

From the last decades, the study of nanoliquids attained notable implication because of its usages in the industry and biological science fields like nanodrug delivery, electromechanical systems, and industrial cooling. The suspension of nanomaterials in carrier liquids yields nanoliquids. The conveyance properties of heat transference are augmented because of the existence of nanoparticles in the fluids like ethylene glycol, kerosene oil, and water. Newly, a liquid called hybrid nanoliquid, a newfangled nanofluid kind, has been applied to progress the heat transference characteristics. These liquids show high heat transference characteristics when compared to nanoliquids. The hybrid nanofluids have many applications in power production engines, solar cells, cooling devices, transportation, defense, medical, microfluidics, and naval structures. Stimulated by these applications, Jayadevamurthy *et al.*[1] numerically explored the bioconvective stream of a hybrid nanofluid past a moving rotating disk with activation energy. Gowda *et al.*[2] explored the particle deposition on the unsteady flow of liquid with suspended Manganese and Nickel zinc ferrite nanoparticles past a moving disk with rotation. Kumar *et al.*[3] inspected the magnetic dipole effect on hybrid nanoliquid flow on an extending surface with suspended Manganese and Nickel zinc ferrite nanoparticles. Yang *et al.*[4] expounded the ferromagnetic fluid stream with ferrite nanoparticle suspension. Tahir *et al.*[5] elucidated the influence of Newtonian heating on ferromagnetic hybrid nanoliquid stream with $NiZnFe_2O_4$ and $MnZnFe_2O_4$ suspension in the base liquid's engine oil C_8H_{18} and kerosene $C_{10}H_{22}$.

The magnetohydrodynamics (MHD) is one of the thrust fields of current research which deals with the motion of the electrically conducting liquids. It has variety of uses in engineering and science fields, such as geophysics, dispersion of metals, modern metallurgy, MHD generators, and fusion reactors. Marangoni convection appears because of surface tension gradients. Liquid–fluid boundaries can produce Marangoni interface layer. Recently, advanced classes of liquids are essential to grasp more effectual performance. This phenomenon has a variety of uses in nanotechnology, atomic reactor, silicon wafers, and semiconductor processing. Stimulated by these applications, several investigators examined the MHD Marangoni convective streams of diverse liquids. Recently, Mahdy *et al.*[6] inspected the Dufour and Soret effects on the MHD stream of liquid with Marangoni convection. Khaled[7] explored the radiation effect on MHD flow of liquid over a flat geometry with Marangoni convection. Chaudhary and Kanika[8] elucidated the MHD stream of nanofluid on a disk with Marangoni convection. Lin and Yang[9] deliberated the MHD radiative stream of liquid above a disk with chemical reaction and Marangoni convection.

Hayat *et al.*[10] explicated the MHD Marangoni convective stream of second-grade liquid with dissipation effect.

Heat transfer plays a prominent role in many noteworthy applications in several industrial and engineering processes. The effective addition of heat, transforming heat from one place to another, and regulating the heat will stabilize the heat transfer process. The transfer of heat takes place due to various causes like nonuniform heat source/sink, viscous dissipation, and so on. So, the energy equation has been formulated by including all the necessary associated terms which explain the heat transfer features. In addition, radiation effect is incorporated to analyze the heat transfer of viscous fluid flows. These effects have significant uses in space technology and high-temperature processes. Inspired by these uses, Khan *et al.*[11] deliberated the impact of viscous dissipation, radiation, Ohmic heating, and chemical reaction on the MHD stream of micropolar liquid. Waqas *et al.*[12] elucidated the heat sink/source effects on the MHD radiative stream of Jeffrey liquid. Shoaib *et al.*[13] numerically elucidated the encouragement of Joule heating, viscous dissipation, and radiation effects on hybrid nanofluid stream above a disk. Iqbal *et al.*[14] explicated the heat sink/source and radiation effect on the viscoelastic liquid flow. Upreti *et al.*[15] illustrated the inhomogeneous heat sink/source and radiation effect on the nanoliquid stream instigated by a stretchy geometry.

The fluid stream with activation energy has a significant role in several industrial fields. The idea of activation energy was first presented by Arrhenius in 1889. It is the minimum quantity of energy which is essential for the species to convert the reactants into products. This phenomenon has noteworthy applications in oil emulsions, fluid mechanics, geothermal and chemical engineering fields. In view of these, Kalaivanan *et al.*[16] explicated the encouragement of activation energy on second-grade liquid streams with radiation effect. Ahmad and Nadeem[17] inspected the domination of activation energy on radiative flow of hybrid nanoliquid. Irfan *et al.*[18] elucidated the impact of activation energy on Carreau nanoliquid flow with nonlinear heat sink/source, radiation, and mixed convection effects. Reddy *et al.*[19] explicated the MHD stream of hybrid nanofluid above a disk with activation energy. Khan[20] discussed the behavior of hybrid nanoparticles in the flow of viscous liquid toward a stretched surface of the disk.

Nowadays, entropy generation is the subject of diverse interests in some territories analogous to combustions, propulsion ducts, electric cooling, turbomachinery, and rotating disk reactors. Entropy production has several uses in solar energy collectors, cooling of modern electronic systems, and cooling of nuclear fuel rods. The mass transfer via thermal gradient is called as Soret effect or thermal diffusion. However, heat transference via concentration gradient is called as Dufour effect or diffusion-thermo. These effects have significant applications in petrology, geothermal energy, hydrology, and nuclear waste disposal. Inspired by these applications, several researchers examined entropy production in the diverse fluid streams over different surfaces with Soret and Dufour effects. Kefayati[21] explicated the entropy production in Power-law fluids with Dufour and Soret effects. Freidoonimehr *et al.*[22] elucidated the entropy production in MHD stream of a fluid above a disk with Dufour and Soret effects. Qayyum *et al.*[23] expounded the entropy production in nonlinear radiative stream among porous disks with Soret, nonlinear heat sink/source, viscous dissipation, and Dufour effects. Khan *et al.*[24] scrutinized the entropy production in MHD stream of viscous liquid with Dufour, thermal radiation, and Soret effects. Jawad *et al.*[25] elucidated the entropy production in MHD stream of Maxwell nanoliquid Dufour, velocity slip, thermal radiation, and Soret effects.

In this work, we examined the entropy production in MHD Marangoni convective stream of hybrid nanofluid with the encouragement of viscous dissipation, nonlinear heat sink/source, thermal radiation, and Soret and Dufour effects.

2. Statement

Steady incompressible 2D flow over stretching sheet is considered here. Nanofluid flow is studied with Manganese Zinc ferrite and Nickle Zinc ferrite ($\mathrm{MnZnFe_2O_4} - \mathrm{NiZnFe_2O_4}$) as nanoparticles and engine oil ($\mathrm{C_8H_{18}}$) as base fluid. Nonlinear effects of radiation, viscous dissipation, and nonlinear heat generation absorption effects are incorporated in the heat equation. Soret and Dufour effects are also taken into account. Entropy generation and Bejan number for Marangoni effect of hybrid nanofluid are examined and discussed. MHD and Darcy–Forchheimer effects are also analyzed. After all these assumptions, we get the following equations:

$$\frac{\partial u}{\partial x} + \frac{\partial v}{\partial y} = 0, \tag{1}$$

$$u\frac{\partial u}{\partial x} + v\frac{\partial u}{\partial y} = \frac{\mu_{hnf}}{\rho_{hnf}}\frac{\partial^2 u}{\partial y^2} - \frac{\upsilon_{hnf}}{K^*}u - Fu^2 - \frac{\sigma^0 B_0^2 u}{\rho_{hnf}}, \tag{2}$$

$$\begin{aligned} u\frac{\partial T}{\partial x} + v\frac{\partial T}{\partial y} = {} & \frac{k_{hnf}}{(\rho c_p)_{hnf}}\frac{\partial^2 T}{\partial y^2} + \frac{\mu_{hnf}}{(\rho c_p)_{hnf}}\left(\frac{\partial u}{\partial y}\right)^2 \\ & + \frac{16\sigma^*}{3(\rho c_p)_{hnf}k^*}\left(3T^2\left(\frac{\partial T}{\partial y}\right)^2 + T^3\frac{\partial^2 T}{\partial y^2}\right) \\ & + D_T\frac{\partial^2 C}{\partial y^2} + Q_0\frac{T_0 - T_\infty}{(\rho c_p)_{hnf}}\exp\left(\frac{-n}{L}y\right) + Q_l\frac{(T - T_\infty)}{(\rho c_p)_{hnf}}, \end{aligned} \tag{3}$$

$$u\frac{\partial C}{\partial x} + v\frac{\partial C}{\partial y} = D\frac{\partial^2 C}{\partial y^2} + D_h\frac{\partial^2 T}{\partial y^2} - k_0^2(C - C_\infty)\left(\frac{T}{T_\infty}\right)^{n^*}\exp\left[\frac{-E_a}{\kappa T}\right]. \tag{4}$$

Boundary conditions are as follows:

$$\mu_{nf}\frac{\partial u}{\partial y} = \frac{\partial \sigma}{\partial x} = \sigma_0\left(\gamma_C\left.\frac{\partial C}{\partial x}\right|_{y=0} + \gamma_T\left.\frac{\partial T}{\partial x}\right|_{y=0}\right),$$

$$v = 0, \quad T = T_\infty + T_0 X^2 \quad \text{at } y = 0,$$

$$u \to 0, \quad T \to T_\infty, \quad C \to C_\infty \quad \text{at } y \to \infty, \tag{5}$$

where

$$\sigma = \sigma_0(1 - \gamma_T(T - T_\infty) - \gamma_C(C - C_\infty)), \tag{6}$$

here

$$\gamma_T \text{ is } \left(-\frac{1}{\sigma_0}\frac{\partial \sigma}{\partial T}\right)\Big|_{T=T_\infty} \quad \text{and} \quad \gamma_C \text{ is } \left(-\frac{1}{\sigma_0}\frac{\partial \sigma}{\partial C}\right)\Big|_{C=C_\infty}, \tag{7}$$

in which $(x,\ y)$, $\mu_{hnf}, \rho_{hnf}, \sigma^0,\ B_0,\ (u,v), c_p, k^*, D,\ \sigma^*,\ K^*,\ Q_0, Q_l,\ k_0^2, T, k_{hnf}$, $(\rho c_p)_{hnf}, T_\infty, T_0, C_\infty, C_0, E_a, n,\ D_h,\ D_T,\ \kappa, \sigma, \gamma_T, \gamma_C$ show Cartesian coordinates, dynamic viscosity, density, electrical conductivity, magnetic field strength, velocity vector, specific heat, mean absorption coefficient, species diffusivity, Stefan–Boltzman constant, porous medium permeability, exponential heat source coefficient, thermal heat source coefficient, chemical reaction rate, temperature, thermal conductivity, heat capacitance, ambient temperature, reference temperature, ambient concentration, reference concentration, activation energy coefficient, exponential constant, betoken the coefficients that measure mass fluxes through temperature and concentration gradients, Boltzmann constant, surface tension, and positive constants for temperature and concentration, respectively.

Transformation used in the present flow system is presented as

$$\begin{aligned} &u = \frac{\upsilon_f}{L} X f'(\xi), \quad v = \frac{\upsilon_f}{L} f(\xi), \quad \theta(\xi) = \frac{T - T_\infty}{T_0 X^2}, \quad \phi(\xi) = \frac{C - C_\infty}{C_0 X^2} \\ &\xi = \frac{y}{L}, \quad X = \frac{x}{L}. \end{aligned} \tag{8}$$

Continuity equation is vanished and rest of the equation takes the form

$$\begin{aligned} &\frac{f'''}{(1-\phi_1)^{2.5}(1-\phi_2)^{2.5}A_1} + ff'' - f'^2 \\ &\quad - \frac{\beta}{(1-\phi_1)^{2.5}(1-\phi)^{2.5}A_1} f' - F_r f'^2 - \frac{M}{A_1} f' = 0, \end{aligned} \tag{9}$$

$$\begin{aligned} &\frac{1}{\Pr A_2}\frac{k_{hnf}}{k_f}\theta'' + f\theta' + \frac{\mathrm{Ec}(f'')^2}{(1-\phi_1)^{2.5}(1-\phi_2)^{2.5}A_2} - 2f\theta' \\ &\quad + \frac{R}{\Pr A_2}((((\theta_w - 1)\theta + 1)^3\theta'' + 3((\theta_w - 1)\theta + 1)^2\theta'^2) \\ &\quad + \frac{1}{A_2}(Q_t\theta + Q\exp(-n\xi)) + D_f\phi'' = 0, \end{aligned} \tag{10}$$

$$\frac{1}{\mathrm{Sc}}\phi'' + f\phi' - 2f'\phi + \mathrm{Sr}\theta'' - k_1(1+\delta\theta)^n \exp\left[\frac{-E_1}{1+\delta\theta}\right] = 0. \tag{11}$$

$$f(0)=0,\quad \frac{f''(0)}{(1-\varphi_1)^{2.5}(1-\varphi_2)^{2.5}}=-2(1+r),\quad \theta(0)=1,\quad \phi(0)=1,$$
$$f'(\infty)\to 0,\quad \theta(\infty)\to 0,\quad \phi(\infty)\to 0, \tag{12}$$

Skin friction and Nusselt number in the dimensional form are defined as

$$\left.\begin{aligned} C_{fx}&=\frac{2\tau_w}{\rho_f u_w^2},\\ Nu_x&=\frac{xq_w}{k_f T_0 X^2},\end{aligned}\right\} \tag{13}$$

where

$$\left.\begin{aligned} \tau_w&=\mu_{hnf}\left.\frac{\partial u}{\partial y}\right|_{y=0},\\ q_w&=-k_{hnf}\left.\frac{\partial T}{\partial y}\right|_{y=0}+q_r,\end{aligned}\right\} \tag{14}$$

The dimensionless form is

$$\left.\begin{aligned} C_{fx}\mathrm{Re}^{0.5}&=\frac{1}{(1-\phi_1)^{2.5}(1-\phi_2)^{2.5}}f''(0),\\ Nu_x\mathrm{Re}^{-0.5}&=-\left(\frac{k_{hnf}}{k_f}+R(\theta(\theta_w-1)+1)^3\right)\theta'(0).\end{aligned}\right\} \tag{15}$$

Entropy generation in presence of radiation, viscous dissipation, porosity, and mass transfer irreversibility is presented as

$$\begin{aligned} S_G=&\frac{1}{T_\infty^2}\left(\frac{k_{hnf}}{k_f}+\frac{16\sigma^* T^3}{3k^* k_f}\right)^2\left(\frac{\partial T}{\partial y}\right)^2+\frac{\sigma B_0^2}{T_\infty}u^2+\frac{\mu_{hnf}}{T_\infty K^*}u^2\\ &+\frac{\mu_{hnf}}{T_\infty}\left(\frac{\partial u}{\partial y}\right)^2+\frac{R^* D}{T_\infty}\left(\frac{\partial T}{\partial y}\right)\left(\frac{\partial C}{\partial y}\right)+\frac{R^* D}{C_\infty}\left(\frac{\partial C}{\partial y}\right)^2. \end{aligned} \tag{16}$$

The dimensionless form is given by:

$$\begin{aligned} N_G=&\left(\frac{k_{hnf}}{k_f}+R\right)\delta\theta'^2+\frac{\mathrm{Br}\ \mathrm{Re}}{(1-\phi_1)^{2.5}(1-\phi_2)^{2.5}}(f'')^2\\ &+\mathrm{MBr}f'^2+\beta\mathrm{Br}f'^2+L^*\theta'\phi'+L^*\frac{\delta_1}{\delta}\phi'^2, \end{aligned} \tag{17}$$

Bejan number is defined as the ratio of heat and mass transfer irreversibility over total entropy

$$\mathrm{Be}=\frac{\left(\frac{k_{hnf}}{k_f}+R\right)\delta\theta'^2+L^*\theta'\phi'+L^*\frac{\delta_1}{\delta}\phi'^2}{\begin{gathered}\left(\frac{k_{hnf}}{k_f}+R\right)\delta\theta'^2+\frac{\mathrm{Br}\ \mathrm{Re}}{(1-\phi_1)^{2.5}(1-\phi_2)^{2.5}}(f'')^2\mathrm{MBr}f'^2\\ +\beta\mathrm{Br}f'^2+L^*\theta'\phi'+L^*\frac{\delta_1}{\delta}\phi'^2\end{gathered}}, \tag{18}$$

Table 1. Thermophysical properties of base fluid and nanoparticles.

Physical properties	ρ (kg/m^3)	C_p (J/kgK)	k (W/mK)	Pr
C_8H_{18}	890	1686	0.145	12,900
$MnZnFe_2O_4$	4700	1050	3.9	—
$NiZnFe_2O_4$	4800	710	6.3	—

where

$$\begin{aligned}
A_1 &= \frac{\rho_{hnf}}{\rho_f} = (1-\phi_2)\left[(1-\phi_1) + \phi_1\frac{\rho_{s1}}{\rho_f}\right] + \phi_2\frac{\rho_{s2}}{\rho_f},\\
\mu_{hnf} &= \frac{\mu_f}{(1-\phi_1)^{2.5}(1-\phi_2)^{2.5}},\\
A_2 &= \frac{(\rho Cp)_{hnf}}{(\rho C_p)_f} = (1-\phi_2)\left[(1-\phi_1) + \phi_1\left(\frac{(\rho Cp)_{s1}}{(\rho Cp)_f}\right)\right] + \phi_2\frac{(\rho Cp)_{s2}}{(\rho Cp)_f},\\
\frac{k_{hnf}}{k_{bf}} &= \frac{k_{s_2} + 2k_{bf} - 2\phi_2(k_{bf} - k_{s_2})}{k_{s_2} + 2k_{bf} + \phi_2(k_{bf} - k_{s_2})}, \quad \frac{k_{bf}}{k_f} = \frac{k_{s_1} + 2k_f - 2\phi_1(k_f - k_{s_1})}{k_{s_1} + 2k_f + \phi_1(k_f - k_{s_1})},
\end{aligned} \tag{19}$$

$\beta = \frac{\upsilon_f L^2}{K^* \upsilon_f}$ is inverse Darcy number, $\beta = \frac{\sigma^0 B_0^2 L^2}{\rho_f \upsilon_f}$ is magnetic parameter, $F_r = \frac{C_b}{\sqrt{K^*}}$ is the Forchheimer parameter, $\Pr = \frac{\upsilon_f}{\alpha_f}$ is the Prandtl number, $\frac{16\sigma^* T_\infty^3}{3k_f k^*}$ is radiation parameter, $\mathrm{Sc} = \frac{\upsilon_f}{D_f}$ is the Schmidt number $k_1 = \frac{k_0^2 L^2}{\upsilon_f}$ is the chemical reaction rate coefficient, $Q = \frac{Q_0 L^2}{\upsilon_f (\rho c_p)_f}$ exponential heat source generation parameter, $Q_t = \frac{Q_l L^2}{\upsilon_f (\rho c_p)_f}$ is thermal heat generation parameter, $E_1 = \frac{Ea}{kT_\infty}$ is the activation energy, $\delta = \frac{T_0 X^2}{T_\infty}$ is the temperature difference parameter, $\mathrm{Br} = \frac{\mu \upsilon_f^2}{kT_0 L^2 X^2}$ is Brinkman number, $L^* = \frac{R^* D C_0}{k_f}$ is diffusion parameter, $\mathrm{Ec} = \frac{\upsilon_f X}{LC_p(T_0 X^2)} = \frac{\upsilon_f^2}{C_p {T_0} L^2 X^2}$ is the Eckert number, $\delta_1 = \frac{C_0 X^2}{C_\infty}$ is the concentration difference parameter, $D_f = \frac{C_0 X^2 D_T (\rho c_p)_f}{k_f T_0 X^2}$ is Dufour number, $\mathrm{Sr} = \frac{T_0 X^2 D_b}{D C_0 X^2}$ is Soret number, $\theta_w = \frac{T_0}{T_\infty}$ is temperature ratio parameter, $r = \frac{C_0 \gamma_C}{T_0 \gamma_T}$ is the Marangoni ratio parameter. Table 1 shows the thermophysical properties of nanoparticles and base fluid.

3. Results and Discussions

The key objective of this segment is to scrutinize the physical characteristics of velocity, thermal, concentration entropy generation, and skin friction; Nusselt number against numerous pertinent parameters are deliberated graphically (see Figs. 1–22). To explain the effects of these key parameters on the fluid flow, heat, and mass transfer characteristics, particular efforts have been focused. The governing equations of the model along with associated boundary constraints are reduced to ordinary differential equations. The entire examination is performed by using dual distinctive nanoparticles of ferrites in particular, manganese zinc ferrite ($MnZnFe_2O_4$) and nickel zinc ferrite ($NiZnFe_2O_4$) in carrier liquid, $C_{10}H_{22}$.

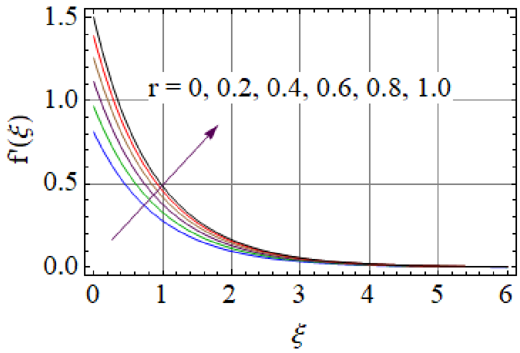

Fig. 1. (Color online) Domination of r on $f'(\xi)$.

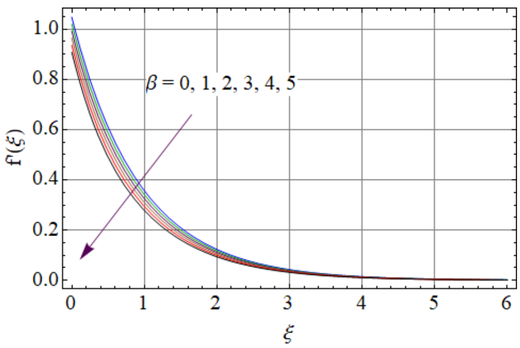

Fig. 2. (Color online) Domination of β on $f'(\xi)$.

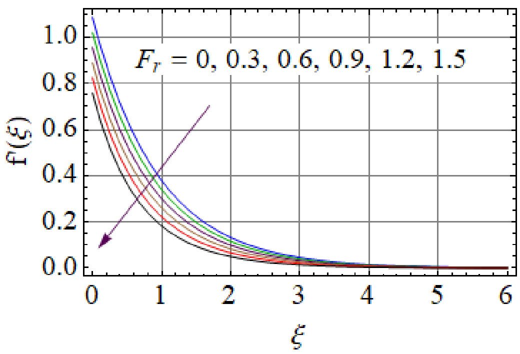

Fig. 3. (Color online) Domination of F_r on $f'(\xi)$.

The thermophysical properties of nanoparticles and carrier liquid are presented in Table 1.

Figures 1–4 highlight the performance of velocity profile for numerous varied parameters, namely, Marangoni ratio, porous parameter, Forchheimer number, and

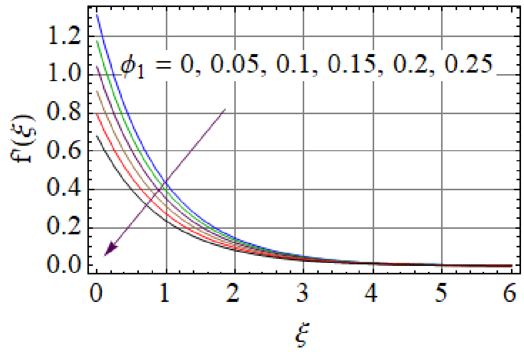

Fig. 4. (Color online) Domination of ϕ_1 on $f'(\xi)$.

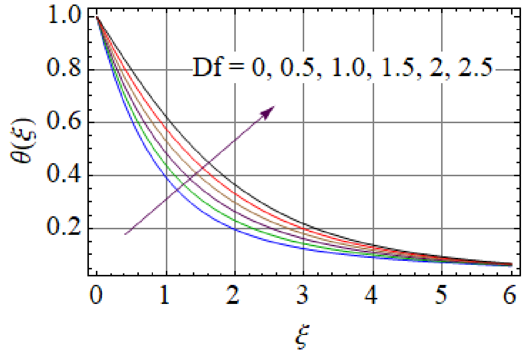

Fig. 5. (Color online) Domination of D_f on $\theta(\xi)$.

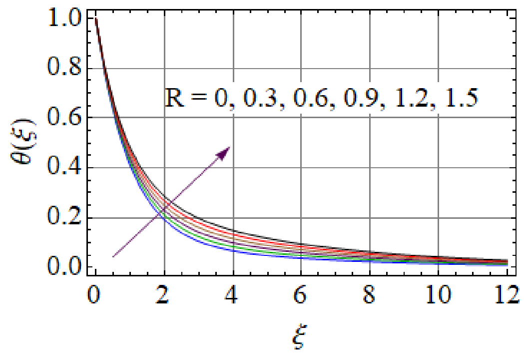

Fig. 6. (Color online) Domination of R on $\theta(\xi)$.

volume fraction. The influence of r on $f'(\xi)$ is exhibited in Fig. 1, which denotes that $f'(\xi)$ enhances with an enhancement of r. Meanwhile the Marangoni effect is a pouring force for liquid stream, a stronger Marangoni effect would almost inevitably increase the velocity gradient. Figure 2 signifies the nature of $f'(\xi)$ for diverse

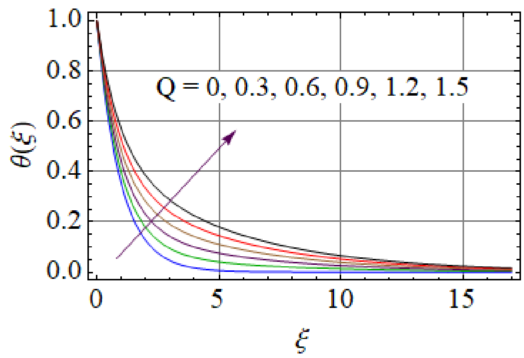

Fig. 7. (Color online) Domination of Q on $\theta(\xi)$.

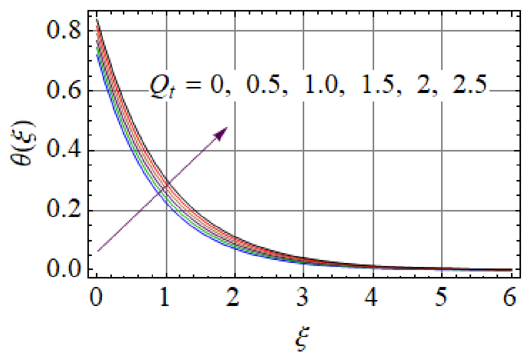

Fig. 8. (Color online) Domination of Q_t on $\theta(\xi)$.

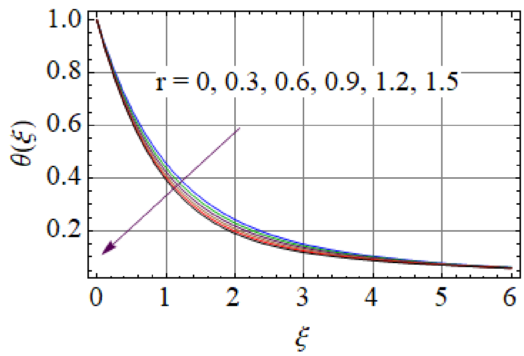

Fig. 9. (Color online) Domination of R on $\theta(\xi)$.

values of β. This figure reveals that $f'(\xi)$ is the declining function of β. Here, with an upsurge of β values, surface drag force inclines, which obviously slowdowns the liquid velocity. The levering of F_r on $f'(\xi)$ is illustrated in Fig. 3. Here, the motion of the fluid reduces significantly for advanced values of F_r. For larger values of F_r,

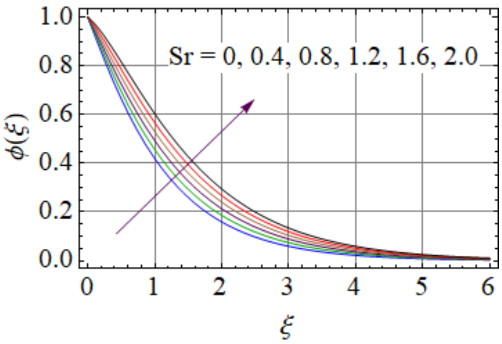

Fig. 10. (Color online) Domination of Sr on $\phi(\xi)$.

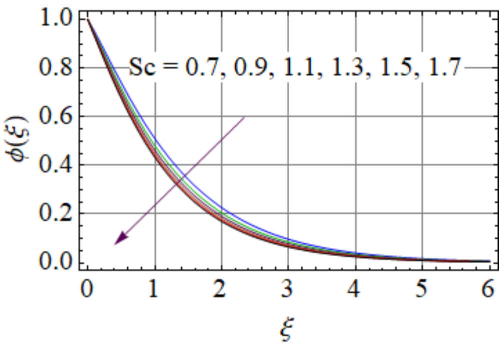

Fig. 11. (Color online) Domination of Sc on $\phi(\xi)$.

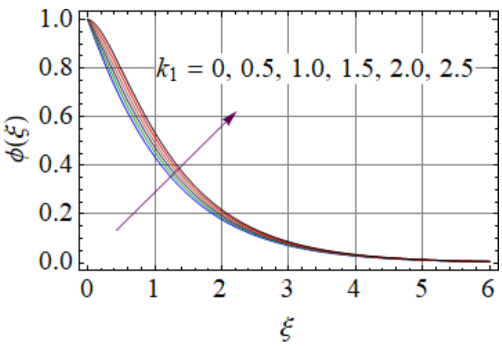

Fig. 12. (Color online) Domination of k_1 on $\phi(\xi)$.

the resistance of fluid particles to flow increases and so velocity decreases. Figure 4 is plotted to denote the major impact of ϕ_1 on $f'(\xi)$. Here, the fluid velocity decreases gradually with an augmentation of ϕ_1.

Variation in temperature profile for numerous values of various dimensionless parameters are portrayed in Figs. 5–9. Figure 5 reveals the behavior of $\theta(\xi)$ for

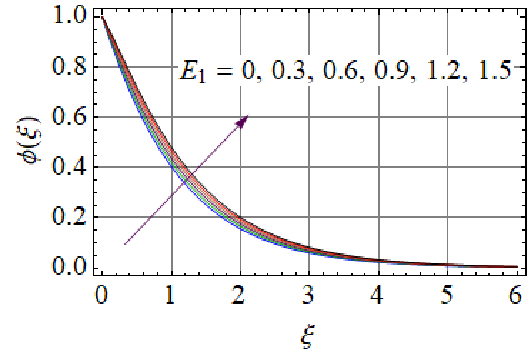

Fig. 13. (Color online) Domination of E_1 on $\phi(\xi)$.

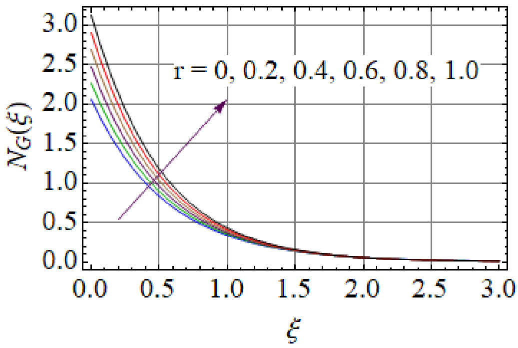

Fig. 14. (Color online) Domination of r on $N_G(\xi)$.

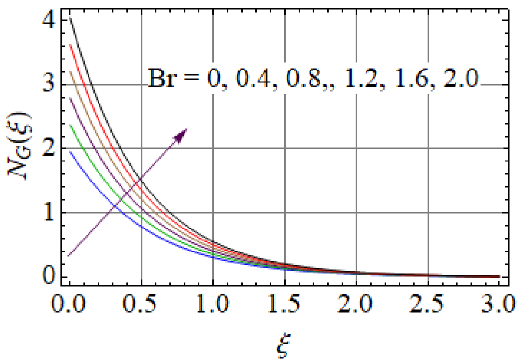

Fig. 15. (Color online) Domination of Br on $N_G(\xi)$.

enhanced values of D_f. Here, $\theta(\xi)$ upsurges rapidly with upsurge in the values of D_f. For greater values of the D_f, an increase in energy flux is observed due to an increase in concentration gradient, which causes temperature to upsurge. The significant consequence of R on $\theta(\xi)$ is elucidated via Fig. 6. In this figure, heightening in the R

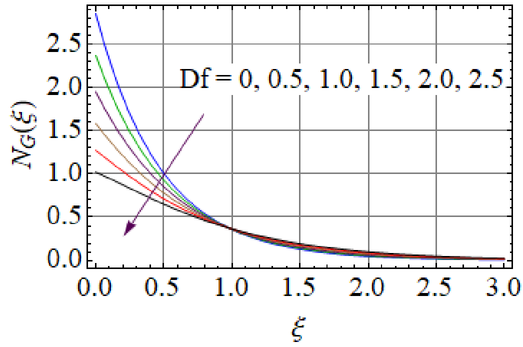

Fig. 16. (Color online) Domination of D_f on $N_G(\xi)$.

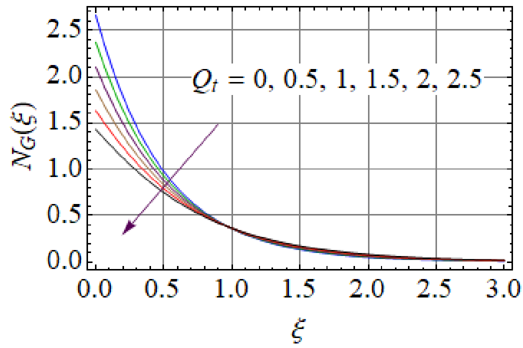

Fig. 17. (Color online) Domination of Q_t on $N_G(\xi)$.

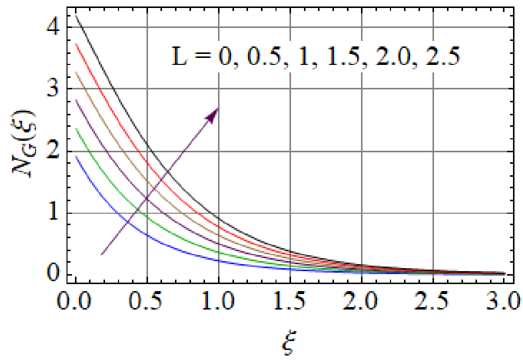

Fig. 18. (Color online) Domination of L on $N_G(\xi)$.

enhances the temperature profile $\theta(\xi)$. Physically, this is because of the decrease in mean absorption coefficient due to higher values of R and its inverse relation with R. So, the thermal gradient and its related boundary layer increase. Figure 7 elucidates the features of $\theta(\xi)$ for various values of Q. Enhancement in Q leads to an upsurge

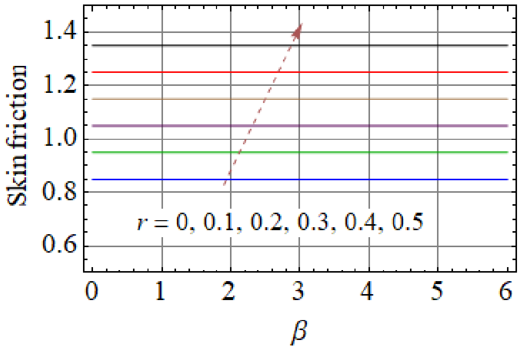

Fig. 19. (Color online) Domination of r on skin friction.

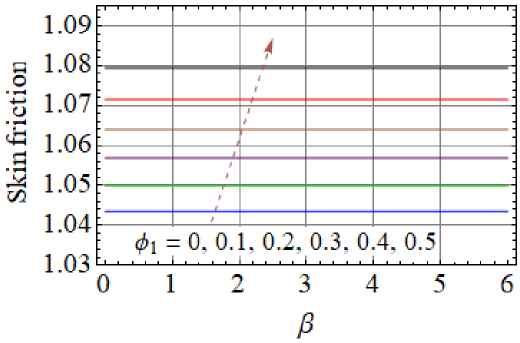

Fig. 20. (Color online) Domination of ϕ_1 on skin friction.

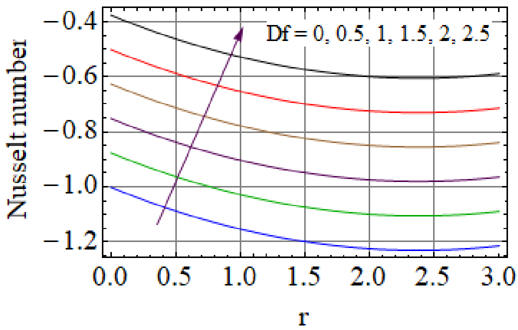

Fig. 21. (Color online) Domination of D_f on Nusselt number.

of $\theta(\xi)$. As the values of Q increased, heat energy moved into the flow direction. As the Q reaches higher values, the temperature profile increases at some point within the boundary layer. In comparison, the thickness of the thermal boundary layer shows a substantial improvement with higher values of the Q. Figure 8 displays the influence of Q_t on $\theta(\xi)$. This figure indicates that $\theta(\xi)$ increases for diverse

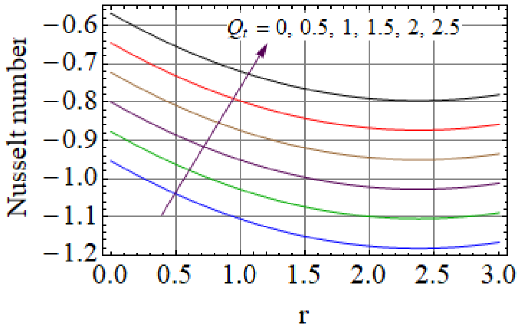

Fig. 22. (Color online) Domination of Q_t on Nusselt number.

values of Q_t. The behavior of temperature profile $\theta(\xi)$ with the influence of r is shown in Fig. 9. It unveils that decreasing nature is observed in $\theta(\xi)$ for improved values of r. Surface stress increases as the r rises, indicating that temperature is low and there is a heavy force of attraction between the surface and the molecules. The levering of diverse dimensionless parameters on concentration distribution is portrayed in Figs. 10–13. Figure 10 indicates the effect of Sr on $\phi(\xi)$. Here, $\phi(\xi)$ enhances with higher values of Sr. This is because of the higher convective flow caused by inclined values of Sr. Hence, $\phi(\xi)$ increases. The nature of $\phi(\xi)$ for varied Sc is portrayed in Fig. 11. As the values of Sc improve, the concentration profile $\phi(\xi)$ reduces rapidly. Mathematically, a dimensionless number relating mass diffusivity with momentum diffusivity yielding a fluid flow is treated as Schmidt number. These two terms are physically called the hydrodynamic thickness layer and mass transport layer. The declination in concentration field due to mass diffusion occurs for an enhancement in the Sc. The effect of k_1 on $\phi(\xi)$ is depicted in Fig. 12. This figure signifies that $\phi(\xi)$ improves for augmentation in k_1 values. The more intense chemical reaction causes nanoparticles to be displaced away from the plate surface and toward the free surface. Physically, the intake of reactive species increases exponentially as k_1 increases. As a consequence, k_1 increases the concentration. Figure 13 explains the feature of $\phi(\xi)$ for various values of E_1. It reveals that $\phi(\xi)$ acts as an increasing function of E_1 and enhances remarkably with an upsurge in E_1 values. Physically, the changed Arrhenius function decays for higher E_1 values, ultimately promoting the multiplicative chemical reaction that decays $\phi(\xi)$. The aspects of r on $N_G(\xi)$ are elucidated in Fig. 14. Here, with an increment in the r values, $N_G(\xi)$ enhances gradually. It demonstrates that as the system's entropy increases, so does the system's entropy. The system's entropy increases as surface tension increases with higher r. The characteristics of $N_G(\xi)$ for increased values of Br are indicated in Fig. 15. This figure unveils that $N_G(\xi)$ increases with an augmentation in the Br values. Brinkman's number controls the release of heat at high temperatures relative to heat transference over molecular conduction. Br is directly related to the production of entropy near the boundary. Moderately high temperatures are produced between layers of fluid-carrying particles, which promote the entropy production. Figure 16 represents the power of D_f on $N_G(\xi)$. Here, $N_G(\xi)$ decreases with an increase in D_f values. The consequence of Q_t on $N_G(\xi)$ is indicated by Fig. 17. Here, an increment in Q_t values leads to the deterioration of Q_t. Figure 18 delineates the aspect of L on $N_G(\xi)$. It denotes that augmentation of $N_G(\xi)$ takes place due to the enhancement of L. Physically, this is due to the escalation of randomness in the system caused by inclined L that causes increment in diffusion rate. The deviation in the skin friction for various values of β with the impact of r is described in Fig. 19. Here, increase in r enhances the skin friction. Figure 20 depicts the variation in the skin friction for various values of ϕ_1. Here, increasing nature is observed in skin friction for enhanced values of ϕ_1. Figure 21 demonstrates the sway of D_f on Nusselt number with various values of r. This figure indicates that Nusselt number exhibits increasing trend for enhancement of D_f. The major variances in the Nusselt number for improved values of Q_t and r are displayed in Fig. 22. Here, Nusselt number increases for enhanced values of both Q_t and r. Here, Nusselt number acts as a declining function of r.

4. Final Remarks

The model is considered for the Soret and Dufour effects on the MHD Marangoni convective stream of liquid with viscous dissipation, nonlinear heat sink/source, and thermal radiation. Further entropy generation is discussed here. The fluctuation in the liquid velocity, thermal, concentration gradient, skin friction, and rate of mass transport for several values of intricate emerging parameters is investigated graphically. The significant conclusions of the present modeling are as follows:

- The upsurge of β values inclines surface drag force which slows down the fluid velocity.
- The fluid velocity decreases gradually with an augmentation of ϕ_1.
- $\theta(\xi)$ increases rapidly with an upsurge in the values of D_f and R.
- The escalating values of Q improve the thermal gradient.
- An increment in the $r$values improves entropy production.
- The entropy production increases with an augmentation in the Br values.
- The decreasing nature is observed in $\theta(\xi)$ for improved values of r.
- The Nusselt number exhibits an increasing trend for enhancement of D_f, Q_t, and r.

Acknowledgments

The authors extend their appreciation to the Deanship of Scientific Research at King Khalid University, Abha 61413, Saudi Arabia, for funding this work through research groups program under Grant Number R.G.P-2/69/41.

References

1. A. Mahdy and S. E. Ahmed, *Eng. Sci. Technol. Int. J* **18** (2015) 24, doi:10.1016/j.jestch.2014.08.003.
2. S. M. Khaled, *Therm. Sci.* **22** (2018) 63.
3. S. Chaudhary and K. M. Kanika, *Phys. Scr.* **95** (2019) 025202, doi:10.1088/1402-4896/ab414c.
4. Y. Lin and M. Yang, *Korean J. Chem. Eng.* **37** (2020) 37, doi:10.1007/s11814-019-0416-6.
5. T. Hayat *et al.*, *J. Mater. Res. Technol.* **9** (2020) 11993, doi:10.1016/j.jmrt.2020.07.067.
6. P. G. R. Jayadevamurthy *et al.*, *Numer. Methods Partial Differ. Equ.*, doi:10.1002/num.22680.
7. R. J. P. Gowda *et al.*, *Surf. Interfaces.* **22** (2021) 100864, doi:10.1016/j.surfin.2020.100864.
8. R. N. Kumar *et al.*, *Phys. Scr.* **96** (2021) 045215, doi:10.1088/1402-4896/abe324.
9. J. Yang *et al.*, *Int. Commun. Heat Mass Transf.* **118** (2020) 104883.
10. H. Tahir *et al.*, *Ain Shams Eng. J.* (2021), doi:10.1016/j.asej.2020.10.026.
11. M. I. Khan *et al.*, *Results Phys.* **7** (2017) 3706, doi:10.1016/j.rinp.2017.09.016.
12. M. Waqas *et al.*, *J. Phys. Chem. Solids.* **133** (2019) 45, doi:10.1016/j.jpcs.2019.03.031.
13. M. Shoaib *et al.*, *Alex. Eng. J.* **60** (2021) 3605, doi:10.1016/j.aej.2021.02.015.
14. S. A. Iqbal *et al.*, *Therm. Sci.* **24** (2020) 1275.
15. H. Upreti *et al.*, *Arab. J. Sci. Eng.* **45** (2020) 7705, doi:10.1007/s13369-020-04826-7.
16. R. Kalaivanan *et al.*, *Case Stud. Therm. Eng.* **22** (2020) 100774, doi:10.1016/j.csite.2020.100774.
17. S. Ahmad and S. Nadeem, *Appl. Nanosci.*, **10** (2020) 5315, doi:10.1007/s13204-020-01334-w.
18. M. Irfan *et al.*, *J. Phys. Chem. Solids.* **125** (2019) 141, doi:10.1016/j.jpcs.2018.10.016.
19. M. G. Reddy *et al.*, *Commun. Theor. Phys.* **73** (2021) 045002, doi:10.1088/1572-9494/abdaa5.
20. M. I. Khan, *Int. Commu. Heat Mass Tran.* **122**, 105177.
21. G. H. R. Kefayati, *Int. J. Heat Mass Tran.* **94** (2016) 582, doi:10.1016/j.ijheatmasstransfer.2015.11.043.
22. N. Freidoonimehr *et al.*, *Entropy* **18** (2016), doi:10.3390/e18050131.
23. S. Qayyum *et al.*, *J. Mol. Liq.* **262** (2018) 261, doi:10.1016/j.molliq.2018.04.010.
24. S. A. Khan *et al.*, *Int. J. Hydrog. Energy* **45** (2020) 14552, doi:10.1016/j.ijhydene.2020.03.123.
25. M. Jawad *et al.*, *Braz. J. Phys.* (2021), doi:10.1007/s13538-020-00835-x.